

Generic Modeling of a Line Commutated HVDC System for Power System Stability Studies

Christoph Hahn^{#1}, Member, IEEE, Anatoli Semerow^{#2}, Matthias Luther^{#3}, Olaf Ruhle^{*4}, Member, IEEE

[#]Chair of Electrical Energy Systems, University of Erlangen – Nuremberg
Konrad-Zuse-Strasse 3-5, 91052 Erlangen, Germany

¹Christoph.Hahn@fau.de

²Anatoli.Semerow@fau.de

³Matthias.Luther@fau.de

^{*}Siemens AG, Sector Infrastructures and Cities SG SE PTI
Freyeslebenstrasse 1, 91058 Erlangen, Germany

⁴Olaf.Ruhle@siemens.com

Abstract— This paper will reveal a novel comprehensive approach for generic modeling and control design of line commutated HVDC systems. The model will be developed based on the essential HVDC equations and transfer functions. Due to comparing the generic model with an EMT (Electro-Magnetic Transient) HVDC model the consistence of the dynamic behavior will be shown.

Furthermore modeling of additional HVDC system facilities like transformer tap-changers and AC filters will be annotated. Control design schemes for line commutated HVDC systems will be derived and the interactions of the controllers applied to the developed model will be investigated.

Keywords— HVDC Generic Modeling, HVDC Control Design, Pole Control, Station Control, HVDC Stability Analysis, Tap-Changer Control, AC Filter Control.

I. INTRODUCTION

Line commutated HVDC systems exist for quite a long time and therefore they are described pretty exactly for example in [1], [2] and [3]. In the past HVDC was generally used to interconnect two different AC systems – e.g. with different frequencies – in order to exchange electrical power in between these AC systems [4].

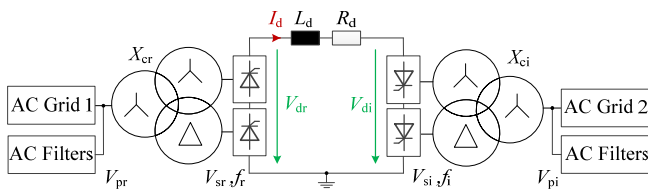


Figure 1: Schematic layout of a twelve-pulse HVDC system

The simplified structure of a twelve-pulse HVDC system is presented in Figure 1. Where X_{cr} and X_{ci} are the short-circuit reactances of the converter transformers, V_{sr} and V_{si} are the AC voltages on the transformer secondary side and V_{pr} and V_{pi} the AC voltages on the primary side respectively; f_r and f_i are the frequencies of the corresponding AC grids, I_d is the direct

current, L_d and R_d are representing the DC line impedance, V_{dr} and V_{di} are the direct voltages at the rectifier and inverter side respectively.

The advantage of twelve-pulse HVDC systems towards six-pulse systems is the decreased emission of harmonics into the AC system [2]. Generally the HVDC transfers electrical power from the rectifier to the inverter side. By the use of voltage reversion it is also possible to transfer electrical power from the inverter to the rectifier side. Since the thyristors have a valve characteristic, current inversion is not practicable. Thus the usage of mass-impregnated cables is often a critical issue [5].

Recently the desire to integrate HVDC systems in yet existing AC networks has gained interest, for example in Germany due to the German Grid Development Plan [6], where the nuclear power plants – mostly located in the south – will be shut down and the upcoming amount of wind power from the North and East Sea wind parks has to be transported to the load centers in Southern Germany. Therefore the AC grid is undersized and an HVDC overlay grid is in discussion.

For so called hybrid AC/DC systems stability analyses are crucial in order to guarantee a secure system operation. Hybrid operation of AC and DC systems is not well established in the global electrical energy supply, since only a couple of countries in the world practice such systems.

In spite of that, analytical models for HVAC/HVDC systems [7] and HVDC stability models [8], [9], [10] were developed; but those are usually designed for small signal analysis and therefore not suitable for a broad operating range which the HVDC has to perform during normal operation in hybrid systems.

For these reasons this paper will show a comprehensive approach in modeling the entire HVDC system including the transmission line, the transformer tap-changers the AC filters and a universal control structure for large signal analysis.

II. HVDC MODELING

This section will describe the modeling process of the entire HVDC system, including the converter, the transmission line, the AC filters and the transformer tap-changer.

A. Converter and Transmission Line Modeling

Based on the schematic equivalent circuit diagram of Figure 1 the basic HVDC equations can be obtained from [1] and are presented in the equations (1) and (2).

$$V_{dr} = B \frac{3\sqrt{2}}{\pi} V_{sr} \cos \alpha_r - B \frac{3}{\pi} X_{cr} I_d \quad (1)$$

$$V_{di} = B \frac{3\sqrt{2}}{\pi} V_{si} \cos \gamma_i - B \frac{3}{\pi} X_{ci} I_d \quad (2)$$

Where α_r is the firing angle of the rectifier, γ_i is the extinction angle of the inverter and the parameter B is one ($B=1$) for six-pulse HVDC systems and B equals two ($B=2$) for twelve-pulse units. Equation (3) represents the dynamic behavior of the transmission line – also illustrated in Figure 1.

$$I_d R_d + L_d \frac{dI_d}{dt} = V_{dr} - V_{di} \quad (3)$$

Since the control system has to provide firing pulses to the inverter based on the firing angle, the extinction angle in equation (2) has to be replaced by the appropriate firing angle:

$$V_{di} = -B \frac{3\sqrt{2}}{\pi} V_{si} \cos \alpha_i + B \frac{3}{\pi} X_{ci} I_d. \quad (4)$$

Due to the replacement of the extinction angle with the appropriate firing angle, the voltage drop caused by the commutation changes its sign [1]. Inserting the equations (1) and (4) in (3) yields:

$$I_d R_d + L_d \frac{dI_d}{dt} = B \frac{3\sqrt{2}}{\pi} (V_{sr} \cos \alpha_r + V_{si} \cos \alpha_i) - B \frac{3}{\pi} I_d (X_{cr} + X_{ci}). \quad (5)$$

In order to obtain a block diagram which represents the dynamic behavior of the system, equation (5) must be transferred to the Laplace domain and solved for the direct current I_d , where s is the Laplace operator:

$$I_d(s) = \underbrace{\left[\frac{B\sqrt{2}}{s \frac{\pi}{3} L_d + \frac{\pi}{3} R_d + B(X_{cr} + X_{ci})} \right]}_{G_{11}(s)} V_{sr}(s) \cdot \cos(\alpha_r(s)) + \underbrace{\left[\frac{B\sqrt{2}}{s \frac{\pi}{3} L_d + \frac{\pi}{3} R_d + B(X_{cr} + X_{ci})} \right]}_{G_{12}(s)} V_{si}(s) \cdot \cos(\alpha_i(s)). \quad (6)$$

It can be easily seen that I_d depends on both the rectifier firing angle $\alpha_r(s)$, the inverter firing angle $\alpha_i(s)$ and the rectifier and inverter side AC voltages respectively. The next step is to establish a relation between the firing angles, the AC voltages and the DC voltage at the inverter. Thus equation (4) needs to be transferred to the Laplace domain. Subsequently the direct current can be replaced by equation (6) which yields an expression for the inverter side DC voltage dependent on the rectifier firing angle $\alpha_r(s)$, the inverter firing angle $\alpha_i(s)$ and the AC voltages V_{sr} and V_{si} respectively.

$$V_{di}(s) = \underbrace{\left[\frac{B^2 \frac{3\sqrt{2}}{\pi} X_{ci}}{s \frac{\pi}{3} L_d + \frac{\pi}{3} R_d + B(X_{cr} + X_{ci})} \right]}_{G_{21}(s)} V_{sr}(s) \cdot \cos(\alpha_r(s)) + \underbrace{\left[\frac{B^2 X_{ci}}{s \frac{\pi}{3} L_d + \frac{\pi}{3} R_d + B(X_{cr} + X_{ci})} - B \right]}_{G_{22}(s)} V_{si}(s) \cdot \cos(\alpha_i(s)). \quad (7)$$

Now the equations (6) and (7) can be summarized which results in the transfer matrix $\mathbf{G}(s)$:

$$\begin{pmatrix} I_d(s) \\ V_{di}(s) \end{pmatrix} = \underbrace{\begin{pmatrix} G_{11}(s) & G_{12}(s) \\ G_{21}(s) & G_{22}(s) \end{pmatrix}}_{\mathbf{G}(s)} \begin{pmatrix} V_{sr}(s) \cdot \cos(\alpha_r(s)) \\ V_{si}(s) \cdot \cos(\alpha_i(s)) \end{pmatrix}. \quad (8)$$

This transfer matrix can be depicted as shown in Figure 2 and constitutes therefore the basis of the generic line commutated HVDC model in the Laplace domain.

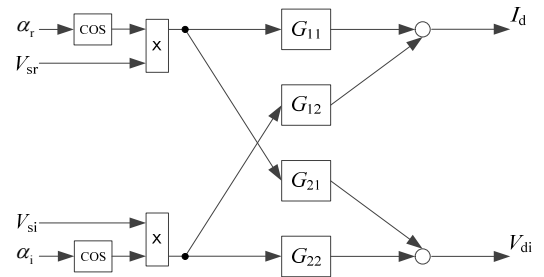


Figure 2: Basic structure of the HVDC model

As Figure 2 shows the HVDC is a coupled system. Firing angles of the rectifier and inverter are influencing both the direct current and the direct voltage. Applying control design to such systems is quite difficult; one opportunity offers the simplification by the usage of a decoupling filter [11].

Changes in the firing angle will not apply immediately to the HVDC system due to the firing delay of 60° on average for six-pulse units and 30° on average for twelve-pulse units [11]. This firing delay equals a dead time element and has to be added to the HVDC model. This dead time element can be linearized and illustrated as a delay first order element with its appropriate transfer function:

$$F_{dr/i}(s) = e^{-sT_{dr/i}} \approx \frac{1}{1 + sT_{dr/i}}, \text{ where } T_{dr/i} = \frac{1}{6B} \frac{1}{f_{r/i}}. \quad (9)$$

The rectifier side DC voltage can now be obtained from the inverter side DC voltage and the transmission line dynamics shown in equation (3). Transferring the converted equation to the Laplace domain reveals the transfer function for $V_{dr}(s)$:

$$V_{dr}(s) = (R_d + sL_d) I_d(s) + V_{di}(s) \quad (10)$$

Consequently the active power at the rectifier and inverter side respectively can be achieved from (6), (7) and (10):

$$P_r = V_{dr} I_d, \quad (11)$$

$$P_i = -V_{di} I_d. \quad (12)$$

For calculating the reactive power consumption of the converters it is mandatory to determine the overlap angle. The current phase shift is not only caused by the firing angles. The overlap angles also contribute to the current delay and therefore play an important role. The overlap angle can be identified by having a closer look to the conducting valves and loops in the converters during a commutation cycle. Solving the differential equations with the appropriate initial conditions yields [1]:

$$u_{r/i} = \arccos\left(\cos(\alpha_{r/i}) - \frac{2\omega I_d L_{cr/i}}{\sqrt{2} V_{sr/i}}\right) - \alpha_{r/i}. \quad (13)$$

Now the rectifier and inverter side reactive power consumption can be represented using the trigonometrical relation to the apparent power [2]:

$$Q_r = P_r \tan\left[\arccos\left(\frac{\cos \alpha_r + \cos(\alpha_r + u_r)}{2}\right)\right], \quad (14)$$

$$Q_i = P_i \tan\left[\arccos\left(\frac{\cos \gamma_i + \cos(\gamma_i + u_i)}{2}\right)\right]. \quad (15)$$

Thereby the extinction angle can be stated as follows:

$$\gamma_{r/i} = 180^\circ - \alpha_{r/i} - u_{r/i}. \quad (16)$$

As the converter and transmission line model were presented in this subsection, the following subsections will describe AC filter and tap-changer modeling respectively.

B. AC Filter Modeling

There are two types of AC filters existing. AC filters for harmonics, which are not further mentioned here since the developed model is designed for power system stability studies and therefore the six- or twelve-pulse converter switching behavior is neglected; consequently no harmonics will occur in this model and hence harmonic filter modeling is not required. The other types of AC filters are used for reactive power compensation.

In the majority of cases AC filters for HVDC systems are dimensioned in order to compensate reactive power in about the size of half of the nominal active power [2]. For this reason the HVDC has a certain amount of filters which are commonly equal sized. Summarized they reveal in the required reactive power for compensation. The reactive power $Q_{ACr/i}$ which is transferred to the respective AC grid is stated in equation (17).

$$Q_{ACr/i} = Q_{r/i} - k \cdot Q_{Fr/i}, \quad (17)$$

where $k \in \{1, \dots, n\}$ and $Q_{Fr/i} = \frac{P_{nr/i}}{2n}$

Where n is the total amount of AC filters belonging to the respective converter station, k is the amount of currently switched filters and $Q_{Fr/i}$ is the reactive power compensation capability of one filter. The energization process can be taken

into account by using a delay first order element which arises from the filter time constant.

C. Transformer Tap-Changer Modeling

Generally the task of a transformer tap-changer is to balance voltage deviations in electrical AC grids which might occur due to load flow changes. This works through the adjustment of the transformer ratio at the high-voltage winding. Commonly the tap-changer is designed to change the nominal transformer voltage in the range from -10...+15% in 1% steps. The primary transformer voltage is adjusted by the AC grid and hence the voltage on the transformer secondary side reveals out of the transformer ratio and the selected tap of the tap-changer:

$$V_{sr/i} = \frac{V_{pr/i}}{r_{r/i}} \cdot (1 + Tap_{r/i}), \quad (18)$$

where $Tap_{r/i} = -0.1 \dots +0.15$ (in 0.01 steps).

Where $r_{r/i}$ is the ratio of the rectifier and inverter side transformer respectively and $Tap_{r/i}$ is the selected tap position. The switching delay of the transformer tap-changer can be taken into account by adding a delay first order element to the tap-changer model.

All these equations, transfer functions and block diagrams respectively were implemented in both the mathematical standard software MATLAB/Simulink[®] and PSS[®]NETOMAC, a program for dynamic network calculation in order to compare the results of the developed generic HVDC model for stability analysis with an EMT HVDC model, which will be shown in section IV.

As all parts of the HVDC system are modeled so far, the next step is to add an appropriate controller unit to the developed model.

III. CONTROL DESIGN

The HVDC control is fundamentally subdivided in two hierarchical levels: the station and pole control. The station control is responsible for the coordination of the requested power of either poles; if it is a bipolar system. Also the AC filter and tap-changer control applies to the station control.

The determined reference values are submitted to the pole control which handles the current, voltage and extinction angle control of the two converters.

A. Pole Control

The pole control is split in the rectifier and inverter control, which are explained in the following subsections.

1) *Rectifier Control*: The basic structure of the rectifier control is illustrated in Figure 3. The input value P_{dref} is selected by the operator and committed by the station control. The minimal value is mostly around 0.1 p.u. of the nominal power in order to avoid intermittent DC current flow. P_{dref} is divided by V_{dr} and hence the reference DC current $I_{dref,P}$ is determined. The time constant T_{dr} is dependent on the operation mode. For the start-up process the delay first order element is much faster than in normal operation mode, whereupon AC failures shouldn't affect the DC current reference value. The VDCOL block (Voltage Dependent Current Order Limitation) limits the power transmission during low voltages by reducing the DC current. This is done by the implementation of a characteristic curve. After the set-

actual comparison and the appropriate PI-controller the arcos block handles the linearization in order to avoid the influence of the cosine terms in equation (6) and (7) to the controller.

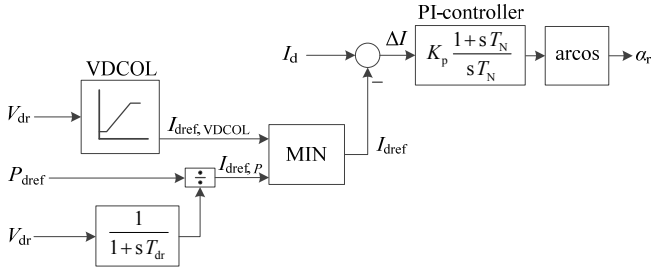


Figure 3: Structure of the rectifier control [5]

2) *Inverter Control*: The basic structure of the inverter control is presented in Figure 4. The inverter control is subdivided in three controllers. During normal operation the inverter operates in voltage control mode. Once an AC voltage drop at the rectifier side occurs, the rectifier won't be able to keep the DC current constant and reaches its limitations. The DC current drops and the power transmission decreases. To avoid a large decrease of the DC current and the transmitted power respectively the inverter has also a current controller. Therefore the reference value of the inverter current controller must be lower than the reference value of the rectifier current controller which is achieved by the designated current margin I_{marg} ; it decreases the DC current reference value typically around 10%.

The CEC block (Current Error Characteristic) contributes with its gain K_{CEC} and the appropriate lead-lag transfer function $C(s)$ to a smooth transition between current and voltage control at the inverter [5].

The extinction angle control intervenes once the actual extinction angle reaches its lower limitation due to the risk of commutation failures. The controller decreases the firing angle and accordingly the extinction angle increases.

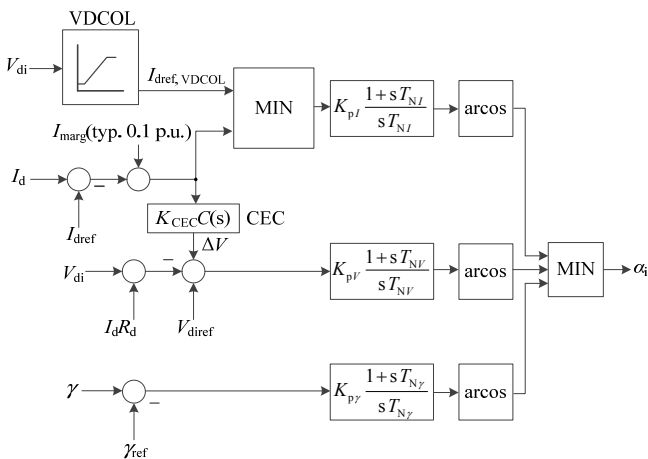


Figure 4: Structure of the inverter control [5]

B. Station Control

The station control is responsible for the coordination of the requested power of either poles and also for the start-up process and the appropriate power ramping.

The AC filter and tap-changer control is also part of the station control. There are different strategies how AC filters and tap-changers can be switched. They will be presented in the following subsections.

1) *AC Filter Control*: The AC filter control includes voltage and reactive power control. The control mode is commonly selected by the operator or preset through a priority list respectively. The first aim of the AC filter control is to keep the AC voltage in its required boundaries. Therefore the actual voltage is compared with its reference value. Once the difference of the actual and reference voltage falls below the lower limit ΔV_{min} , a switching operation of one of the AC filters is applied. The AC voltage will rise up. If the AC voltage is still too low, another AC filter will be switched on after a certain holding time. The similar procedure applies if the AC voltage is too high. Once the upper limit ΔV_{max} is reached, an AC filter will be switched off. This might apply until all AC filters are switched on or off.

The second control mode is the reactive power control. The same principle is used here. If the difference of the actual and reference reactive power is higher as the desired reactive power deviation, an AC filter needs to be switched on or switched off if it is too low. The explained structure is illustrated in Figure 5.

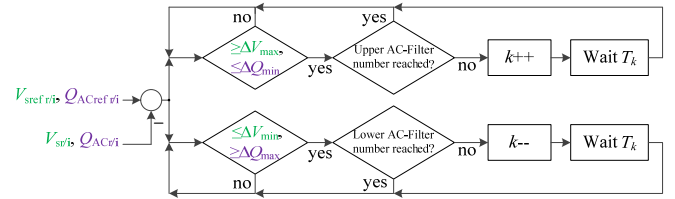


Figure 5: Basic AC filter control structure

2) *Tap-Changer Control*: There exist also two different control modes for the tap-changers. The tap-changer can be used in order to keep the voltage at the secondary side of the transformer constant or to keep the operating point of the HVDC system constant. A constant operating point guarantees a stable power transmission and the requested reserves.

Once the firing angle increases and the difference with its reference value becomes lower than a certain boundary $\Delta \alpha_{\text{min}}$, the tap-changer has to step down in order to decrease the secondary side AC voltage. After the AC voltage decreases the firing angle will decrease in order to keep the DC current or voltage constant. If the firing angle is still too high another tap step will be initialized after a certain holding time.

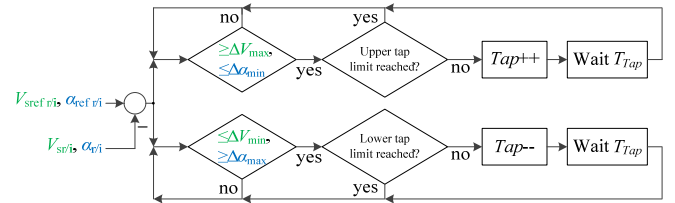


Figure 6: Basic tap-changer control structure

For keeping the AC voltage constant the same principle is used here. Once the voltage drops and becomes lower than a certain limit, the tap-changer has to step up and the voltage

will increase immediately. The basic structure of the tap-changer control is shown in Figure 6.

IV. RESULTS AND COMPARISON WITH AN EMT MODEL

This section will present the results of the HVDC modeling process. Therefore the developed stability model will be compared with an EMT six-pulse HVDC model, which can be found e.g. in the MATLAB/Simulink® Examples Library.

The transfer functions and equations derived in section II were implemented in MATLAB/Simulink® and PSS®NETOMAC, where both tools showed the same results; standard HVDC parameters and controller parameters respectively can be obtained from [12] and [13] and are presented in Table I. Also the EMT HVDC model was implemented in MATLAB/Simulink® using thyristors and other electrical equipment from the SimPowerSystems® Toolbox. The same controlling system – explained in section III – is applied to the EMT HVDC model.

Table I – HVDC parameters for simulation

$V_{pr} = V_{sr}$	200 kV
$V_{pi} = V_{si}$	200 kV
$X_{cr} = X_{ci}$	0.7 Ω
$f_r = f_i$	50 Hz
R_d	0.1 Ω
L_d	0.085 H
V_{diref}	255 kV
I_{dref}	3000 A
γ_{ref}	20°
$K_{p, I, V, \gamma}$	0.4
$T_{N, I, V, \gamma}$	0.01 sec

For the comparison of the developed generic HVDC model with the EMT HVDC model a simple test case under the condition of constant grid voltages was chosen. The results are shown in Figure 7 and Figure 8. The two models start operating at their set point which is classified as the voltages and currents are at their nominal level at 100%, the rectifier works in current control mode and the inverter in voltage control mode. At $t=0.2$ sec the current reference value steps immediately up to 150% and at $t=0.4$ sec the voltage reference value steps down to 50%.

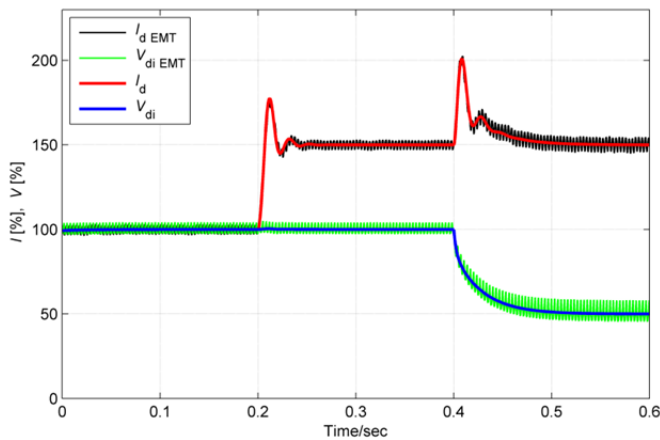


Figure 7: Direct voltages and currents of the EMT and stability HVDC model

Generally it can be seen, that the curves of the EMT HVDC model are less smooth than those of the stability model. Of course the EMT HVDC model takes the six-pulse converter behavior into account; therefore these peaks occur due to the

thyristor switching every 60° on average. As in the HVDC stability model converter switching is not modeled it represents the average DC voltage and current values.

The curves of the two models fit in a broad range; even the dynamics during the transient sequences are generally similar. Small deviations might occur due to the transient converter behavior. Depending on the exact time and angle respectively and the appropriate transient voltages at the converters by the time the thyristors are fired, the current peaks might vary due to different transient operating points; also the phase shift of the two AC grids play a role during these phenomena.

Correspondingly the firing angles of the two models are commonly similar; those are presented in Figure 8.

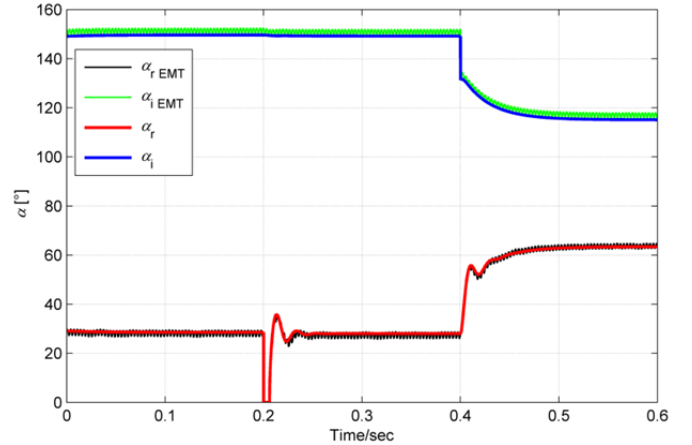


Figure 8: Firing angles of the rectifier and inverter of the EMT and stability HVDC model

In order to show the correct behavior of the entire control scheme an accelerated start-up process of the generic model to the HVDC set point is shown in Figure 9.

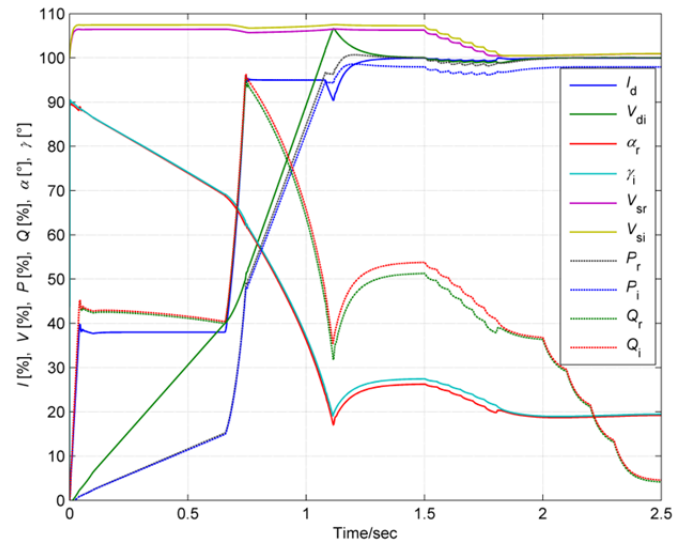


Figure 9: Simulation of an HVDC start-up process with the entire control scheme

The HVDC model was connected to an AC grid on the rectifier and inverter side which is characterized by a high short-circuit level. The grid connection was performed by the use of Three-Phase Dynamic Load blocks.

At the beginning of the simulation all HVDC values start at zero except the rectifier firing angle α_r and the inverter

extinction angle γ_i which start at 90° . The AC-grid voltages are seven and eight percent higher than their nominal values in order to see the influence of the tap-changer control once it is initialized. The station control ramps up the active power reference value with a time constant of one second. The direct voltage reference value is ramped up with the same time constant. As a consequence the reference value of the direct current results out of the division of P_{dref} and V_{dr} (Figure 3). The direct current reaches its first limitation due to the VDCOL (described in section III) at around 38%. Once the direct voltage reaches a certain boundary the VDCOL releases the next limitation and I_d rises further up to around 95%.

During the first 0.7 seconds the reactive power follows the shape of I_d ; once I_d and V_{dr} have almost reached their nominal values the reactive power decreases due to the decrease of the firing and extinction angle respectively (equation (14) and (15)). During the high slope of the reactive power the AC voltages drop slightly.

At around 1.5 sec the start-up process reaches a steady state. At this time the tap-changer control is initialized in voltage control mode. It identifies that the AC voltages are too high and starts decreasing the position of the tap-changers; it stops once the AC voltage reaches 100%.

At $t=2.0$ sec the AC filter control is initialized in reactive power control mode. The aim is to compensate the reactive power of the HVDC system. Therefore the AC filter control successively engages more filters until the reactive power is sufficiently compensated.

After $t=2.5$ sec the HVDC system and its entire control scheme is in a steady state condition. The simulation shows that the start-up process works in accurate way.

V. CONCLUSIONS

This paper depicted the development process of an HVDC model for stability analysis. At first the basic HVDC equations and appropriate transfer functions yield in the inner HVDC model (Figure 2). Based on this structure, further HVDC quantities like active power, reactive power, overlap angle, extinction angle, AC filters and tap-changers could be modeled.

Subsequently the entire HVDC control including the pole control (rectifier and inverter control) and the station control (power, AC filter and tap-changer control) was modeled and added to the HVDC model.

In order to show the correct dynamic behavior of the HVDC model a comparison with an EMT HVDC model was carried out and it was stated that the transient behavior of the stability model fits to an EMT model.

At the end an accelerated HVDC start-up process was demonstrated where all HVDC controllers were involved. It was shown that the HVDC and the appropriate control works authentically regarding its requirements and drives the HVDC system to its desired operating point.

A novel comprehensive approach of modeling the entire HVDC system and its appropriate control was shown in this paper. This approach comprises modeling of the entire HVDC system and its control schemes for large signal analysis, including detailed simulations.

REFERENCES

- [1] E. W. Kimbark, *Direct Current Transmission*. John Wiley & Sons, New York, London, Sydney, Toronto, 1971.
- [2] J. Arrillaga, *High Voltage Direct Current Transmission*. The Institution of Engineering and Technology, London (UK), 2008.

- [3] K. R. Padiyar, *HVDC Power Transmission Systems*. New Academic Science Limited, Kent (UK), 2011.
- [4] B. M. Buchholz, D. Povh and D. Retzmann, "Stability Analysis for large Power System Interconnections in Europe," *IEEE Power Tech*, St. Petersburg, Russia, June 2005.
- [5] V. Crastan and D. Westermann, *Electrical power supply III, (Elektrische Energieversorgung III)*. Springer publishing, Berlin Heidelberg, Germany, 2012 (in German).
- [6] O. Feix, R. Obermann, M. Strecker and A. Brötel, "German grid development plan, (Netzentwicklungsplan Strom 2013)", *The German Transmission System Operators*, Berlin, Germany, March 2013 (in German).
- [7] D. Jovcic, N. Pahalawaththa and M. Zavahir, "Analytical Modelling of HVDC-HVAC Systems," *IEEE Transactions on Power Delivery*, Vol. 14, No. 2, April 1999.
- [8] R. M. Brandt, U. Annakkage, D. Brandt and N. Kshatriya, "Validation of a Two-Time Step HVDC Transient Stability Simulation Model including Detailed HVDC Controls and DC Line L/R Dynamics," *IEEE Power Engineering Society General Meeting*, Montreal, Canada, June 2006.
- [9] E. v. Person, "Calculation of transfer functions in grid-controlled converter systems. With special reference to h.v. d.c. transmissions," *IEEE Proceedings of the Institution of Electrical Engineers*, Vol. 117, No. 5, May 1970.
- [10] P. F. de Toledo, *Modeling and control of a line-commutated HVDC transmission system interacting with a VSC STATCOM, Doctoral Dissertation: Royal Institute of Technology*. Department of Electrical Engineering, Stockholm (Sweden), 2007.
- [11] C. Hahn, A. Müller and M. Luther, "A novel approach to select HVDC - controller parameters by using a decoupling filter," *International Conference on Renewable Energies and Power Quality (ICREPO'13)*, Bilbao, Spain, March 2013.
- [12] F. Yang and Z. Xu, "An approach to Select PI Parameters of HVDC Controllers," *Power Engineering Society General Meeting*, Montreal, Québec, Canada, June 2006.
- [13] T. Rae, E. Boje, G. D. Jennings and R. G. Harley, "Controller structure and design of firing angle controllers for (unit connected) HVDC systems," *4th IEEE Africon Conference*, Stellenbosch, South Africa, September 1996.

BIOGRAPHIES



Christoph Hahn received his Dipl.-Ing. degree from the University of Erlangen-Nuremberg, Germany, in 2011. Currently he is a Ph.D. student and research associate at the Chair of Electrical Energy Systems at the University of Erlangen-Nuremberg, Germany. His research interests lie in the field of HVDC modeling and control.



Anatoli Semerow received his B.Eng. degree in 2009 from the University of Applied Sciences of Hannover, Germany, and his M.Sc. degree in 2011 from Technical University of Clausthal, Germany. Since 2011 he has been working as a research associate at the University of Erlangen-Nuremberg, Germany. His research interests are related to Power System Stability and Dynamics.



Matthias Luther studied electrical engineering and received his Ph.D. at the Technical University of Brunswick, Germany in 1992. From 1993 he held different functions and management positions in the electricity industry at PreussenElektra, E.ON Netz and TenneT TSO. Since 2011 he is professor and holds the Chair of Electrical Energy Systems at the University of Erlangen-Nuremberg, Germany.



Olaf Ruhle received his Dipl.-Ing. and his Ph.D. degree in electrical engineering from the Technical University of Berlin in 1990 and 1994 respectively. Since 1993 he is a member of Power Transmission and Distribution Group and the system planning department at Siemens in Erlangen, Germany. He is responsible for the program system PSS[®]NETOMAC support, sale and training worldwide. He is visiting professor at several universities.